INORGANIC CHEMISTRY FRONTIERS

RESEARCH ARTICLE

View Article Online
View Journal | View Issue

Check for updates

Cite this: *Inorg. Chem. Front.*, 2023, **10**, 3230

An ultra-stable Cu^{I}_{12} cluster built from a Cu^{I}_{6} precursor sandwiched by two Cu^{I}_{3}-thiacalixarene units for efficient photothermal conversion†

Zuohu Zhou, Linmeng Xu, Guiyan Zhao,* Kun Zhou, Baokuan Chen and Yanfeng Bi *

Received 15th March 2023,
Accepted 24th April 2023

DOI: 10.1039/d3qi00479a

rsc.li/frontiers-inorganic

Published on 25 2023. Downloaded on 25-08-2025 22:57:58.

We report the synthesis, crystal structure, optical properties, and photothermal conversion properties of an ultra-stable cuprous Cu_{12} cluster, namely $\{[Cu^{I}_{3}(HTC4A)]_2[Cu^{I}_{6}(2\text{-}PyS)_6]\}\cdot H_2O$ (**Cu_{12}**, H_4TC4A = *p-tert*-butylthiacalix[4]arene, 2-PySH = 2-pyridinethiol), which was built from a pre-synthesized $Cu^{I}_{6}(2\text{-}PyS)_6$ (**Cu_6**) precursor and two Cu^{I}_{3}-HTC4A polynuclear secondary building units (PSBUs). The **Cu_{12}** cluster features a sandwich-like framework in which the Cu_6 core is double surface capped by forming six Cu–S bonds with two Cu^{I}_{3}-HTC4A PSBUs. The "cluster–cluster" assembly strategy enables all the metal centers in the **Cu_{12}** cluster to be monovalent and efficient organic ligand protection makes the cuprous cluster stable in common solvents (alcohol, acetonitrile, acetone, $CHCl_3$, *N N*-dimethylacetamide, *etc.*) as well as in strong acids (pH = 1) or bases (pH = 14). Band gap determination and photophysical analysis combined with density functional theory (DFT) calculations indicated that Cu^{I}_{3}-HTC4A PSBUs can tune the electron and hole distribution of the Cu_6 core, which makes **Cu_{12}** a stable and efficient photothermal conversion material both in the solid state and in water/*N*,*N*-dimethylformamide solvents.

1 Introduction

Coinage metal clusters with atomically precise structures are of great interest due to their fascinating structure evolution and promising applications in biological sensing, catalysis, and nanoscale optoelectronics.[1–3] Coinage metal clusters can be synthesized by reduction growth, seed growth, alloying, and ligand exchange methods.[4] A variety of huge coinage clusters, including Cu_{81},[5] Au_{279},[6] and Ag_{490},[7] have been successfully synthesized and structurally determined. Compared with the achievements in synthesis, the utilization of coinage metal clusters is limited by their stability at ambient condition. Due to their unique potential applications in catalytic,[8] luminescence,[9] and biological processes[10] and of course, due to their atom economy, cuprous clusters have received considerable attention from scientists. However, copper has a lower reduction potential than Au^{I} and Ag^{I} and is not readily stable in air; thus, it is always challenging to fabricate a stable cuprous cluster that can be utilized under ambient or extreme conditions.[11–13] The ligand modification and protection strategy has been proven to be an effective way to fabricate stable cuprous clusters, and ligands with rich electronic structures can also endow these clusters with a variety of applications.[14–16]

Cyclic calixarene compounds with high thermal and chemical stability as well as changeable conformations and abundant coordination sites have received extensive attention in coordination chemistry.[17] *p-tert*-Butylthiacalix[4]arene (H_4TC4A) is the most utilized calixarene with sulfur bridging. It has been proven to be an especially effective ligand to form M_x (TC4A) (M = Mn^{II}, Co^{II}, Ni^{II}, Fe^{II}, *etc.*, x = 3 or 4) polynuclear secondary building units (PSBUs) by strongly combined coordination of bridging S atoms and phenoxo groups for the assembly of metal clusters.[18–22] Recently, Wang and Sun used H_4TC4A to assemble a series of Au^{I} and Ag^{I} clusters, and the ligand protection to achieve stable clusters is evident.[23–28] It is also familiar to the assembly of Cu^{II}-based metal clusters but there are limited examples of pure Cu^{I} clusters of H_4TC4A that can be obtained. Liao and co-workers reported a two-dimensional (2D) polymer based on $Cu^{I}_{2}Cl_2$-(TC4A) units.[29] However, this compound is easily turned into a Cu^{II}_{4}-(TC4A) cluster in the mother liquid in air. Attempts at H_4TC4A functionalization, *e.g.*, *t*-butyl substituted by phenyl groups or –OH replaced by –SH, did not work to separate a stable Cu^{I}-(H_4TC4A) compound at ambient condition.[29,30] Therefore, the

School of Petrochemical Engineering, Liaoning Petrochemical University, Fushun, Liaoning 113001, P. R. China. E-mail: gyzhao@lnpu.edu.cn, biyanfeng@lnpu.edu.cn

†Electronic supplementary information (ESI) available: Experimental details, DFT calculations, and additional figures and tables. CCDC 2246463. For ESI and crystallographic data in CIF or other electronic format see DOI: https://doi.org/10.1039/d3qi00479a

This journal is © the Partner Organisations 2023

Published on 25 2023. Downloaded on 25-08-2025 22:57:58.

absence of Cu^{II} species in the initial synthesis system might be the determining factor in the fabrication of the stable Cu^{I} compound H_4TC4A. Otherwise, H_4TC4A tends to use its multidentate coordination sites to form a triangular coordination environment, leaving at least two active metal orbitals to be coordinated, as is favorable for forming Cu^{II} compounds.[31–36] Very recently, two isomeric $Cu^{I}_{13}(TC4A)_2$ pairs were successfully isolated by using Cu^{II} and Cu^{0} sources, and the $NaBH_4$ reduction agent was applied to avoid the reoxidation of the Cu^{I} species by O_2 in air.[26]

In this work, we adopted a "cluster–cluster" assembly strategy to control the synthesis of a cuprous **Cu_{12}** cluster by presynthesis of a $[Cu^{I}_6(2\text{-PyS})_6]$ (2-PySH = 2-pyridinethiol) precursor with exposed S coordination sites and capped with Cu^{I}_3-HTC4A PSBUs afterward. The **Cu_{12}** cluster was stable at ambient condition for six months and the broad absorbance makes it an excellent photothermal conversion material both in the solid state and in solvents.

2. Experimental section

2.1 Materials and measurements

p-tert-Butylthiacalix[4]arene (H_4TC4A) was synthesized according to the procedure in the literature.[37] Other reagents were purchased commercially without further purification. Thermogravimetric analysis (TGA) was carried out at a ramp rate of 10 °C min^{-1} in an N_2 flow with a TA Q600 TGA analyzer. Fourier transform infrared spectroscopy (FT-IR) using KBr pellets was performed on a PerkinElmer Spectrum GX spectrometer. Powder X-ray diffraction (PXRD) was performed using a Bruker D8 VENTURE diffractometer with Cu-Kα radiation. Ultraviolet–visible (UV-vis) spectra were recorded on an Agilent Cary5000 spectrometer. X-ray photoelectron spectroscopic (XPS) measurements were made with an ESCALAB 250Xi using a monochromic Al K_αX-ray source (1486.6 eV).

2.2 Synthesis of a $Cu^{I}_6(2\text{-PyS})_6$ (2-PySH = 2-pyridinethiol) precursor

$Cu^{I}_6(2\text{-PyS})_6$ (**Cu_6**) is a known compound and was synthesized by the solvothermal method in this report.[38] X-ray diffraction measurements showed the same crystal parameters as those in the literature. Details of the structure solution and final refinements are given in Table S1.† The phase purity of the crystals was confirmed by powder X-ray diffraction (PXRD) analysis.

2.3 Synthesis of $\{[Cu^{I}_3(HTC4A)]_2[Cu^{I}_6(2\text{-PyS})_6]\}\cdot H_2O$ (Cu_{12})

A mixture of **Cu_6** (0.050 g, 0.05 mmol), CuCl (0.030 g, 0.3 mmol), H_4TC4A (0.72 g, 0.1 mmol), three drops of triethylamine, methanol (MeOH, 5.0 mL), and *N*,*N*-dimethylacetamide (DMA, 5.0 mL) in a 20 mL Teflon-lined autoclave was kept at 130 °C for two days and then slowly cooled to 20 °C. Light brown block crystals were obtained in 34.7% yield (based on H_4TC4A). The crystals were isolated by filtration and then washed with 1 : 1 MeOH–DMA and dried in air. FT-IR (KBr pellet, cm^{-1}): 3440(m), 2962(s), 1636(w), 1577(s), 1451(s), 1358(m), 1311(m), 1257(s), 1124(s), 885(m), 831(m), 752(s), and 720(m).

2.4 Single crystal X-ray diffraction

Intensity data were collected at 296 K using Mo-K_α radiation on a Bruker D8 QUEST system (λ = 0.71073 Å). Direct methods were used to solve the crystal structures, and then full-matrix least squares on F^2 (SHELXTL-2014) were used to refine them.[39] All non-hydrogen atoms were polished anisotropically except for lattice water. The hydrogen atoms in the organic ligands were theoretically fixed on the particular atoms and refined isotropically with predetermined thermal factors. The hydrogen atoms on solvent H_2O molecules were directly incorporated in the molecular formula. Details of the structure solution and final refinements for the compounds are given in Table S1.† CCDC2246463 contains the supplementary crystallographic data for this paper.†

3. Results and discussion

3.1 Synthesis and characterization

The **Cu_6** precursor was synthesized by the solvothermal method (Fig. 1). **Cu_{12}** was built from one Cu_6 core with a similar arrangement to that of the **Cu_6** precursor and two Cu^{I}_3-HTC4A (H_4TC4A = *p-tert*-butylthiacalix[4]arene, Fig. S1†) polynuclear secondary building units (PSBUs) by the "cluster–cluster" assembly strategy. The phase purity of the samples is confirmed by the powder X-ray diffraction (PXRD) of the two clusters, which consisted of the simulated patterns obtained from single-crystal X-ray diffraction (SCXRD, Fig. S2†). The FT-IR results revealed the predicted peaks for the components of **Cu_{12}**, showing the characteristic C–H vibration *p-tert*-butyl groups and phenolic groups of H_4TC4A (Fig. S3†). TGA tests were performed to test the thermal stability and the TGA residue is also confirmed by PXRD (Fig. S4 and S5†).

3.2 Crystal structures

Single-crystal X-ray diffraction showed that 2-PyS^- ligands in **Cu_6** show the same coordination mode (μ_3-$\kappa_N{}^1$:$\kappa_S{}^2$) and copper centers are tri-coordinated with one N and two μ_2-S atoms. **Cu_{12}** crystallizes in the tetragonal system with the space group $P4_2/mbc$. The **Cu_{12}** cluster is a sandwich-like structure with a $Cu_6(2\text{-PyS})_6$ core double-surface capped by two Cu_3-HTC4A PSBUs by forming six Cu–S bonds (Fig. 1). The $Cu_6(2\text{-PyS})_6$ core in **Cu_{12}** is an inheritance from the **Cu_6** precursor except for the 2-PyS^- ligands in a different coordination mode (μ_4-$\kappa_N{}^1$:$\kappa_S{}^3$). Furthermore, each $HTC4A^{3-}$ ligand bonds with three Cu centers (Cu1, Cu2, and $Cu1^{i}$) and each Cu is coordinated by two μ_2 phenoxyl atoms and one bridging sulfur atom from the $HTC4A^{3-}$ ligand. The overall coordination of three Cu in PSBUs is four-coordination in a tetrahedral arrangement. All the Cu atoms both in **Cu_6** and **Cu_{12}** showed the low coordination (2, 3, 4) of a typical Cu^{I}.[26,29,30,40,41] Both **Cu_6** and **Cu_{12}** contain a highly similar $Cu_6(2\text{-PyS})_6$ core but differ in distortion. The average Cu···Cu distance in the "$Cu_6(2\text{-PyS})_6$ core" of

Published on 25 2023. Downloaded on 25-08-2025 22:57:58.

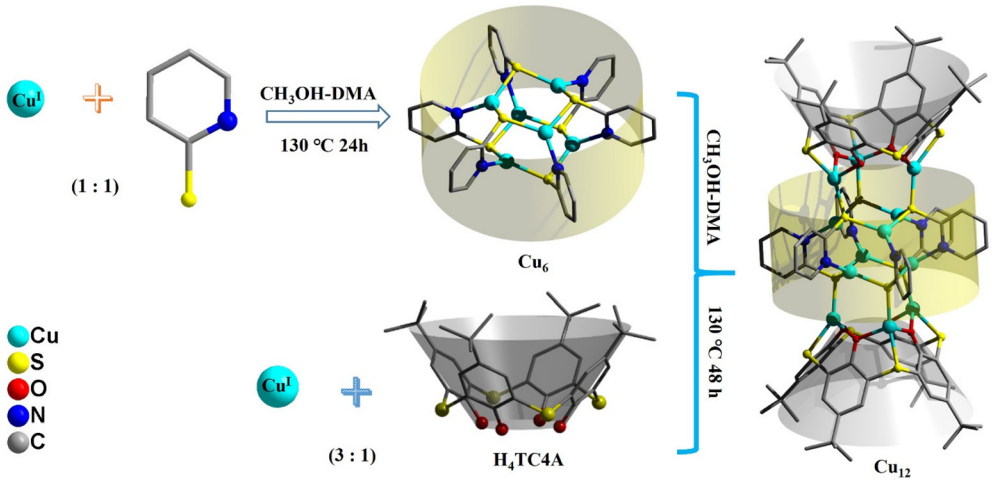

Fig. 1 Synthesis and structure of Cu_6 and Cu_{12}.

Cu_{12} being 3.251 Å is much larger than that for Cu_6 (2.953 Å), which suggests that the presence of Cu_3-HTC4A stretched the "$Cu_6(2\text{-PyS})_6$ core" on both sides (Fig. 2). Additionally, the distance between two adjacent coppers (Cu1···Cu2, Cu1···Cu3^{iii}, Cu2···Cu3^{iii}) was 3.605, 3.437, and 3.622 Å, respectively (Fig. S6†). Combined with the Cu coordination, bond valence calculation, charge balance (Table S2†) and X-ray photoelectron spectroscopy (XPS) results (Fig. S7†), all the Cu in Cu_{12} being cuprous is evident. Additionally, no obvious interaction is observed between adjacent two metal clusters and isolated solvent waters are located in the crystal lattice of Cu_{12} (Fig. S8†).

3.2 Stability of Cu_{12}

We tested the stability of Cu_{12} under various conditions. The crystal samples were immersed in water solutions with pH values of 1, 7, and 14 for 48 h, in 1 M H_2O_2 for 6 h, and in common solvents (or mixture) for 48 h. Then, PXRD patterns were obtained under ambient conditions. As shown in Fig. 3, the tested PXRD patterns are well-matched with the simulated one from SCXRD. Additionally, Cu_{12} can also keep its crystallinity well after exposing to air for more than six months. All those results suggested the outstanding structural integrity and stability of Cu_{12}.

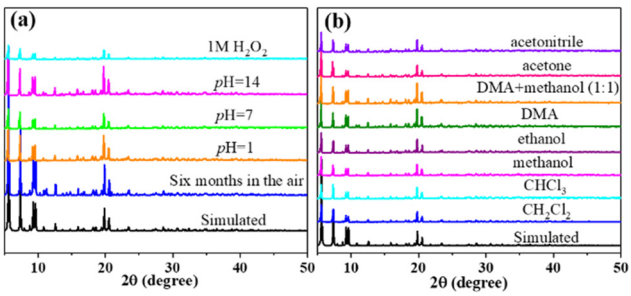

Fig. 3 PXRD pattern of Cu_{12} showing the stability under different conditions: (a) in air and water solution; (b) in common organic solvents.

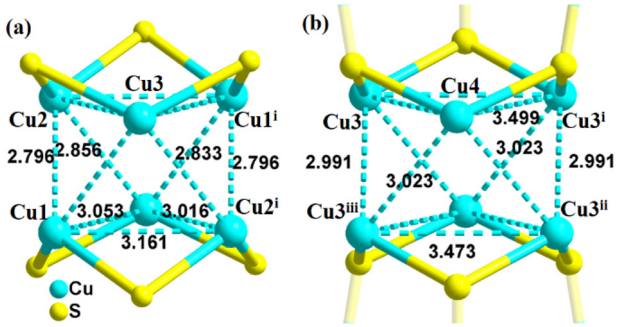

Fig. 2 (a) Cu···Cu distance (Å) in Cu_6 and (b) Cu···Cu distance (Å) in the "$Cu_6(2\text{-PyS})_6$" core of Cu_{12}. Symmetry codes: Cu_6 (i) $-x+1, -y+1, -z+1$; Cu_{12} (i) $x, y, -z+1$; (ii) $-x+1, -y+1, -z+1$; (iii) $-x+1, -y+1, z$.

For most cluster coordination compounds, it is easy to lose the crystallinity under ambient conditions and their crystal structures are usually determined at low temperatures by liquid nitrogen protection, especially for those containing coinage metals.[5–7,42] The high-resolution XPS spectrum of S in Cu_{12} is 1.3 eV bigger than that in Cu_6, which suggests that the electron density of S is lower in Cu_{12} than in Cu_6 (Fig. 4). It is more likely that the strong coordination and delocalization ability of HTC4A^{3-} tunes the S electron density distribution from the $Cu_6(2\text{-PyS})_6$ core to Cu_3^I-HTC4A PSBUs, which corresponded to the high-resolution XPS spectra of Cu 2p (Fig. S7b†). That is, HTC4A^{3-} contributes to the stability of Cu_{12} by not only shielding Cu^I from oxidation, but also changing the electron distribution to decrease the activity of the Cu_{12}^I core.

3.3. UV–vis absorption and DFT calculation studies

The solid-state UV–vis spectra of Cu_6 and Cu_{12} were tested in the range of 200–800 nm (Fig. 5). The absorption of Cu_{12} is weaker in the range of 400–500 nm and stronger between

 This journal is © the Partner Organisations 2023

Published on 25 2023. Downloaded on 25-08-2025 22:57:58.

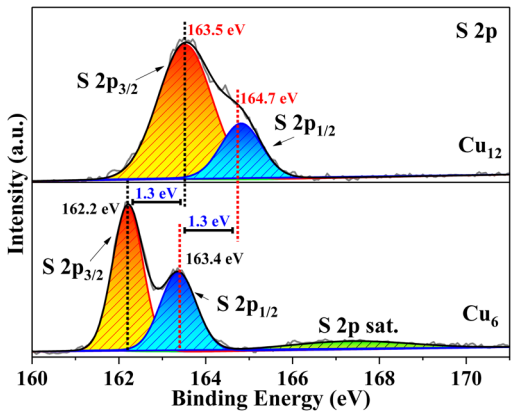

Fig. 4 High-resolution XPS spectra of S 2p (Cu_{12} and Cu_6).

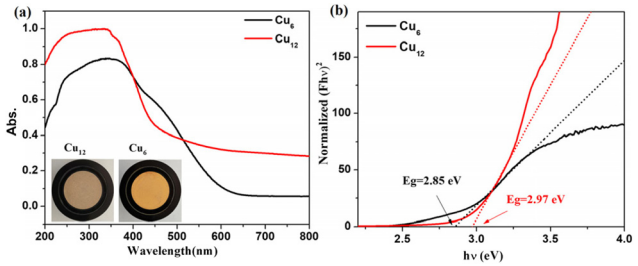

Fig. 5 (a) UV-vis spectra and (b) band gaps of Cu_6 and Cu_{12}.

200–400 nm compared with Cu_6, the latter of which might be due to the presence of $HTC4A^{3-}$, which enhances the $\pi \rightarrow \pi^*$ transformation of Cu_{12}.[43,44] The broad absorption in 500–800 nm indicated that Cu_{12} might be a good candidate as a long-wavelength responsive light material. To better understand the relationship between the compound structures and their light absorption, DFT calculations using B3LYP were performed for Cu_6 and Cu_{12} based on the models from single-crystal structures, respectively (Fig. 6). Both the HOMO and HOMO−1 of Cu_{12} are almost entirely located on the calixarene ligand (donor), while the LUMO is mainly located on the

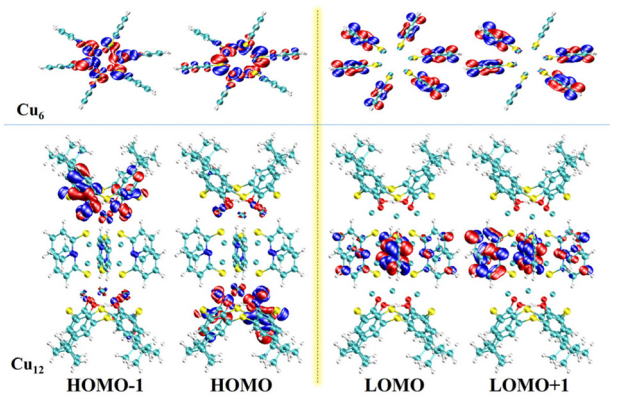

Fig. 6 Frontier molecular orbitals of Cu_6 (top) and Cu_{12} (bottom).

"$Cu_6(2\text{-PyS})_6$" core (acceptor). This suggests that ligand-to-metal charge transfer (LMCT) and ligand-to-ligand charge transfer (LLCT) might occur and result in long-wavelength light absorption.[45] Contrastingly, the HOMO and HOMO−1 of Cu_6 are virtually totally found on the Cu center, whereas the LUMO and LUMO+1 are primarily placed on the ligand, indicating metal-to-ligand charge transfer (MLCT) being the main contribution that results in the 400–500 nm absorption.[45] Simultaneously, the HOMO–LUMO gap with the B3LYP function and the def2-SVP basis group for Cu_{12} and Cu_6 are calculated to be 2.96 eV and 3.61 eV, respectively, the former of which is quite accordant with that from the band gap determination (2.97 eV) while the latter of which is obviously different (2.85 eV). As for the DFT calculations performed on single clusters excluding "cluster–cluster" interactions, the difference between the HOMO–LUMO gap and band gap for Cu_6 is contributed to the inter-cluster actions *via*, for example, π···π or C–H···π interactions of two 2-PyS^- ligands from two clusters (Fig. S9†). The larger band gap energy and non-inter-cluster actions make Cu_{12} not only stable in the crystalline form, but also in a single cluster.

3.4 Photothermal studies

Photothermal studies on Cu-based coordination compounds mainly involved divalent[46] and mixed valence[41,47–49] clusters, and a pure Cu^I analogue is rarely involved. The larger band gaps originated from LMCT and LLCT as well as the ultra-stable nature of Cu_{12} prompted us to investigate the photothermal properties. An appropriate sample was placed on a 2 × 2 cm^2 glass sheet, a 660 nm laser was used as a light source, and a thermal imager recorded the temperatures of the sample. The irradiation power was 0.4 W cm^{-2} (see the ESI† for details). The time–temperature plots were obtained as shown in Fig. 7a. The temperature of Cu_{12} sharply increased from room temperature (20 °C) to 70 °C within 5 s corresponding to a 9.2 °C s^{-1} heating rate. In stark contrast, the temperatures of Cu_6 and the mixture (H_4TC4A:CuCl = 1 : 3) reached 27 °C and 26 °C, with the heating rate of 1 °C s^{-1} and

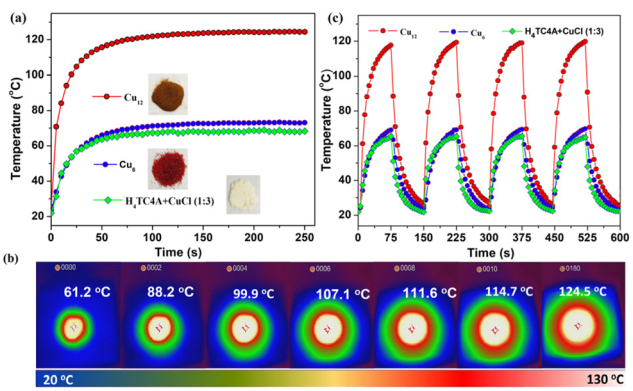

Fig. 7 Photothermal experiment in the solid state: (a) time–temperature curves for Cu_{12}, Cu_6, and the mixture; (b) photothermal images for Cu_{12} (interval, 5 s); (c) light on–off cycles.

Published on 25 2023. Downloaded on 25-08-2025 22:57:58.

0.8 °C s^{-1}, respectively, under the same conditions. The maximum temperature of **Cu_{12}** reached 124.5 °C (Fig. 7b) and was kept steady; however, the temperatures were significantly lower (below 73.1 °C) for both **Cu_6** and the mixture. No obvious decay was observed in four light on–off cycles for three compounds (150 s per cycle, Fig. 7c). A fast photothermal conversion rate and a visual photothermal delay were apparent for **Cu_{12}**. It is indicated that **Cu_{12}** has efficient photothermal conversion properties compared with the contrasts. With combined absorption properties and DFT calculation, the superior photothermal conversion of **Cu_{12}** might originate from the larger absorption at 660 nm and LMCT nature, which results in electron–hole pairs relaxing to the band edges upon irradiation and then releasing phonon energy to transform into heat through a nonradioactive decay.[50] For better comparison, some recent reports on Cu-based coordination compounds/representative composites for photothermal conversion are listed in Table S3.†

Cu_{12} is insoluble and stable in H_2O or DMF as indicated by PXRD experiments. By placing the **Cu_{12}** sample at the bottom of a plastic pipe in different solvents and exposing the sample to a 0.4 W cm^{-2} 660 nm laser, the solvent photothermal property for the metal cluster was evaluated (Fig. 8). Upon irradiation within 10 min, the solid sample temperature elevated quickly from room temperature to 65.7 °C in DMF and 56.5 °C in H_2O. Meanwhile, the solvent also gradually warmed to 43.3 °C and 29.9 °C, respectively. The solid sample temperatures were similar while the solvent temperatures were different. The different photothermal conversion properties in H_2O and DMF are due to the different solvent heat capacities. After the experiment, the samples were separated from the solvents by filtration and characterized by PXRD. The resulting PXRD patterns still matched the simulated one (Fig. S10†). The results suggest that **Cu_{12}** is stable even after the photothermal experiments involving the solvent.

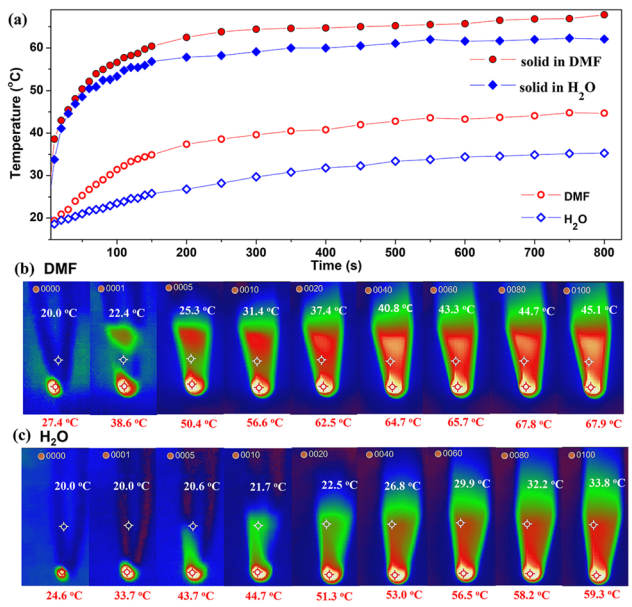

Fig. 8 Photothermal experiment in solvent for **Cu_{12}** (a) time–temperature curves; photothermal images in DMF (b) and H_2O (c). Red and white labels represent sample and solvent temperatures.

4. Conclusions

An ultra-stable cuprous **Cu_{12}** cluster has been fabricated by the "cluster–cluster" assembly strategy from pre-synthesized $Cu_6^I(2\text{-PyS})_6$ and two Cu_3^I-HTC4A polynuclear secondary building units (PSBUs). The modification of $Cu_6^I(2\text{-PyS})_6$ with two Cu_3^I-HTC4A PSBUs not only makes the obtained sandwich-like **Cu_{12}** cluster stable in air, in strong acids, or bases as well as in common solvents, but also significantly tunes the light absorption. **Cu_{12}** showed improved photothermal conversion efficiency and stability both in the solid state and in solvents, which is quite correlated with the band gap structure as evidenced by DFT calculations. This work provides a new view of fabricated stable cuprous materials and may shed light on the utilization of solar energy for storage and conversion.

Author contributions

Y. F. Bi and B. K. Chen conceived and designed the project. Z. H. Zhou, L. M. Xu, G. Y. Zhao, and K. Zhou performed the experiments and characterization. Z. H. Zhou performed the DFT calculations and wrote the original draft. G. Y. Zhao and Y. F. Bi provided supervision, validated the experimental results, and reviewed and edited the manuscript. B. K. Chen and Y. F. Bi provided funding support.

Conflicts of interest

There are no conflicts to declare.

Acknowledgements

This work was supported by the National Natural Science Foundation of China (no. 91961110, 22171122).

References

1 J. P. Wilcoxon and B. L. Abrams, Synthesis, structure and properties of metal nanoclusters, *Chem. Soc. Rev.*, 2006, **35**, 1162.
2 S. Yamazoe, K. Koyasu and T. Tsukuda, Nonscalable Oxidation Catalysis of Gold Clusters, *Acc. Chem. Res.*, 2014, **47**, 816–824.
3 R. Jin, Atomically precise metal nanoclusters: stable sizes and optical properties, *Nanoscale*, 2015, **7**, 1549–1565.

 This journal is © the Partner Organisations 2023

Published on 25 2023. Downloaded on 25-08-2025 22:57:58.

4 Q.-F. Yao, T.-K. Chen, X. Yuan and J.-P. Xie, Toward Total Synthesis of Thiolate-Protected Metal Nanoclusters, *Acc. Chem. Res.*, 2018, **51**, 1338–1348.

5 R.-W. Huang, J. Yin, C. Dong, A. Ghosh, M. J. Alhilaly, X. Dong, M. N. Hedhili, E. Abou-Hamad, B. Alamer, S. Nematulloev, Y. Han, O. F. Mohammed and O. M. Bakr, $[Cu_{81}(PhS)_{46}(^tBuNH_2)_{10}(H)_{32}]^{3+}$ Reveals the Coexistence of Large Planar Cores and Hemispherical Shells in High-Nuclearity Copper Nanoclusters, *J. Am. Chem. Soc.*, 2020, **142**, 8696–8705.

6 N. A. Sakthivel, S. Theivendran, V. Ganeshraj, A. G. Oliver and A. Dass, Crystal Structure of Faradaurate-279: Au_{279}(SPh-^{t}Bu)$_{84}$ Plasmonic Nanocrystal Molecules, *J. Am. Chem. Soc.*, 2017, **139**, 15450–15459.

7 C. E. Anson, A. Eichhöfer, I. Issac, D. Fenske, O. Fuhr, P. Sevillano, C. Persau, D. Stalke and J. Zhang, Synthesis and Crystal Structures of the Ligand-Stabilized Silver Chalcogenide Clusters $[Ag_{154}Se_{77}(dppxy)_{18}]$, $[Ag_{320}(S\mathit{t}Bu)_{60}S_{130}(dppp)_{12}]$, $[Ag_{352}S_{128}(StC_5H_{11})_{96}]$, and $[Ag_{490}S_{188}(StC_5H_{11})_{114}]$, *Angew. Chem., Int. Ed.*, 2008, **47**, 1326–1331.

8 Y. Zhang, L.-Z. Dong, S. Li, X. Huang, J.-N. Chang, J.-H. Wang, J. Zhou, S.-L. Li and Y.-Q. Lan, Coordination environment dependent selectivity of single-site-Cu enriched crystalline porous catalysts in CO_2 reduction to CH_4, *Nat. Commun.*, 2021, **12**, 6390.

9 W.-T. Wei, Y.-Z. Lu, W. Chen and S.-W. Chen, One-Pot Synthesis, Photoluminescence, and Electrocatalytic Properties of Subnanometer-Sized Copper Clusters, *J. Am. Chem. Soc.*, 2011, **133**, 2060–2063.

10 A. Wüst, L. Schneider, A. Pomowski, W. G. Zumft, P. M. H. Kroneck and O. Einsle, Nature's way of handling a greenhouse gas: the copper-sulfur cluster of purple nitrous oxide reductase, *Biol. Chem.*, 2012, **393**, 1067–1077.

11 T. A. D. Nguyen, Z. R. Jones, B. R. Goldsmith, W. R. Buratto, G. Wu, S. L. Scott and T. W. Hayton, A Cu_{25} Nanocluster with Partial Cu(0) Character, *J. Am. Chem. Soc.*, 2015, **137**, 13319–13324.

12 A. Ghosh, R.-W. Huang, B. Alamer, E. Abou-Hamad, M. Nejib, O. F. Mohammed and O. M. Bakr, $[Cu_{61}(S^tBu)_{26}S_6Cl_6H_{14}]$+: A Core–Shell Superatom Nanocluster with a Quasi-*J*36 Cu_{19} Core and an "18-crown-6" Metal-Sulfide-like Stabilizing Belt, *ACS Mater. Lett.*, 2019, **1**, 297–302.

13 S. G. Bratsch, Standard Electrode Potentials and Temperature Coefficients in Water at 298.15 K, *J. Phys. Chem. Ref. Data*, 1989, **18**, 1–21.

14 X. Kang and M.-Z. Zhu, Intra-cluster growth meets inter-cluster assembly: The molecular and supramolecular chemistry of atomically precise nanoclusters, *Coord. Chem. Rev.*, 2019, **394**, 1–38.

15 Q. Tang, G.-X. Hu, V. Fung and D. Jiang, Insights into Interfaces, Stability, Electronic Properties, and Catalytic Activities of Atomically Precise Metal Nanoclusters from First Principles, *Acc. Chem. Res.*, 2018, **51**, 2793–2802.

16 L.-C. Liu and A. Corma, Metal Catalysts for Heterogeneous Catalysis: From Single Atoms to Nanoclusters and Nanoparticles, *Chem. Rev.*, 2018, **118**, 4981–5079.

17 M. W. Hosseini, Thia-, Mercapto-, and Thiamercapto-Calix[4]arenes in *Calixarenes 2001*, ed. Z. Asfari, V. Böhmer, J. Harrowfield, J. Vicens and M. Saadioui, Kluwer Academic Publishers, Dordrecht, 2002, pp. 110–129.

18 Y.-F. Bi, S.-C. Du and W.-P. Liao, Thiacalixarene-based nanoscale polyhedral coordination cages, *Coord. Chem. Rev.*, 2014, **276**, 61–72.

19 X.-X. Hang and Y.-F. Bi, Thiacalix[4]arene-supported molecular clusters for catalytic applications[J], *Dalton Trans.*, 2021, **50**, 3749–3758.

20 X.-X. Hang, B. Liu, X.-F. Zhu, S.-T. Wang, H.-T. Han, W.-P. Liao, Y.-L. Liu and C.-H. Hu, Discrete $\{Ni_{40}\}$ Coordination Cage: A Calixarene-Based Johnson-Type (J_{17}) Hexadecahedron, *J. Am. Chem. Soc.*, 2016, **138**, 2969–2972.

21 H.-T. Han, L. Kan, P. Li, G.-S. Zhang, K.-Y. Li, W.-P. Liao, Y.-L. Liu, W. Chen and C.-H. T. Hu, 4.8 nm Concave $\{M_{72}\}$ (M=Co, Ni, Fe) metal-organic polyhedra capped by 18 calixarenes, *Sci. China: Chem.*, 2021, **64**, 426–431.

22 D.-T. Geng, X. Han, Y.-F. Bi, Y.-C. Qin, Q. Li, L.-L. Huang, K. Zhou, L.-J. Song and Z.-P. Zheng, *Chem. Sci.*, 2018, **9**, 8535–8541.

23 Z. Wang, H.-F. Su, Y.-W. Gong, Q.-P. Qu, Y.-F. Bi, C.-H. Tung, D. Sun and L.-S. Zheng, A hierarchically assembled 88-nuclei silver-thiacalix[4]arene nanocluster, *Nat. Commun.*, 2020, **11**, 308.

24 Z. Wang, F. Alkan, C. M. Aikens, M. Kurmoo, Z. Zhang, K. Song, C. Tung and D. Sun, An Ultrastable 155—Nuclei Silver Nanocluster Protected by Thiacalix[4]arene and Cyclohexanethiol for Photothermal Conversion, *Angew. Chem., Int. Ed.*, 2022, **61**, e202206742.

25 L.-L. Zhang, D.-W. Liang, Y. Wang, D. Li, J.-H. Zhang, L. Wu, M.-K. Feng, F. Yi, L.-Z. Xu, L.-D. Lei, Q. Du and X.-J. Tang, Caged circular siRNAs for photo-modulation of gene expression in cells and mice, *Chem. Sci.*, 2018, **9**, 44–51.

26 C.-K. Zhang, Z. Wang, W.-D. Si, L.-Y. Wang, J.-M. Dou, Z.-Y. Gao, C.-H. Tung and D. Sun, Solvent-Induced Isomeric Cu_{13} Nanoclusters: Chlorine to Copper Charge Transfer Boosting Molecular Oxygen Activation in Sulfide Selective Oxidation, *ACS Nano*, 2022, **16**, 9598–9607.

27 Z. Wang, L. Li, L. Feng, Z.-Y. Gao, C.-H. Tung, L.-S. Zheng and D. Sun, Solvent–Controlled Condensation of $[Mo_2O_5(PTC4A)_2]^{6-}$ Metalloligand in Stepwise Assembly of Hexagonal and Rectangular Ag_{18} Nanoclusters, *Angew. Chem., Int. Ed.*, 2022, **61**, e202200823.

28 Z. Wang, H.-F. Su, L.-P. Zhang, J.-M. Dou, C.-H. Tung, D. Sun and L. Zheng, Stepwise Assembly of Ag_{42} Nanocalices Based on a Mo^{VI}-Anchored Thiacalix[4]arene Metalloligand, *ACS Nano*, 2022, **16**, 4500–4507.

29 Y.-F. Bi, W.-P. Liao, X. Wang, R.-P. Deng and H.-J. Zhang, Self–Assembly from Two–Dimensional Layered Networks to Tetranuclear Structures: Syntheses, Structures, and Properties of Four Copper–Thiacalix[4]arene Compounds, *Eur. J. Inorg. Chem.*, 2009, **2009**, 4989–4994.

Published on 25 2023. Downloaded on 25-08-2025 22:57:58.

30 N. Frank, A. Dallmann, B. Braun-Cula, C. Herwig and C. Limberg, Mercaptothiacalixarenes Steer 24 Copper(I) Centers to form a Hollow–Sphere Structure Featuring Cu_2S_2 Motifs with Exceptionally Short Cu...Cu Distances, *Angew. Chem.*, 2020, **132**, 6801–6805.

31 Q.-L. Guo, W.-X. Zhu, S. Gao, S.-L. Ma, S.-J. Dong and M.-Q. Xu, A novel 2D coordination polymer based on a copper(II) tetramer with *p*-sulfonated thiacalix[4]arene, *Inorg. Chem. Commun.*, 2004, **7**, 467–470.

32 G. Karotsis, S. Kennedy, S. J. Dalgarno and E. K. Brechin, Calixarene supported enneanuclear Cu(ii) clusters, *Chem. Commun.*, 2010, **46**, 3884.

33 F.-J. Li and R.-J. Sa, Formation of $Cu_{3,4}$(TCA), making the TCA complex a highly selective probe for Cu^{2+} detection: a TDDFT study, *J. Mater. Chem. C*, 2019, **7**, 2443–2456.

34 R. E. Fairbairn, R. McLellan, R. D. McIntosh, M. A. Palacios, E. K. Brechin and S. J. Dalgarno, Oxacalix[4]arene-supported di-, tetra- and undecanuclear copper(II) clusters, *Dalton Trans.*, 2014, **43**, 5292–5298.

35 T. Kajiwara, N. Kon, S. Yokozawa, T. Ito, N. Iki and S. Miyano, Synthesis, Structure, and Ferromagnetic Behavior of Decacopper(II) Cluster Complex Supported by Hexaanionic p - tert- Butylthiacalix[6]arene, *J. Am. Chem. Soc.*, 2002, **124**, 11274–11275.

36 Y.-F. Bi, W.-P. Liao and H.-J. Zhang, Assembly of Supramolecular Compounds with Water-Soluble Calix[4]arenes, *Cryst. Growth Des.*, 2008, **8**, 3630–3635.

37 N. Iki, C. Kabuto, T. Fukushima, H. Kumagai, H. Takeya, S. Miyanari, T. Miyashi and S. Miyano, Synthesis of *p-tert*-Butylthiacalix[4]arene and its Inclusion Property, *Tetrahedron*, 2000, **56**, 1437–1443.

38 S. Kitagawa, M. Munakata, H. Shimono, S. Matsuyama and H. Masuda, Synthesis and Crystal Structure of Hexanuclear Copper(I) Complexes of 3-Pyridine-2-thionate, *J. Chem. Soc., Dalton Trans.*, 1990, 2105–2109.

39 G. M. Sheldrick, Crystal structure refinement with *SHELXL*, *Acta Crystallogr., Sect. B: Struct. Sci.*, 2015, **71**, 3–8.

40 Y. Fang, W.-X. Xie, K. Han, K. Zhou, L. Kang, J. Shi, B.-K. Chen and Y.-F. Bi, Diphosphine modified copper(I)-thiacalixarene supramolecular structure for effective photocurrent response and photodegradation of methylene blue, *Polyhedron*, 2022, **222**, 115934.

41 D.-N. Yu, Z.-X. Yao, F. Bigdeli, X.-M. Gao, X. Cheng, J.-Z. Li, J.-W. Zhang, W. Wang, Z.-J. Guan, Y. Bu, K.-G. Liu and A. Morsali, Synthesis and Study of Photothermal Properties of a Mixed-Valence Nanocluster Cu^{I}/Cu^{II} with Strong near-Infrared Optical Absorption Supported by 4-*tert*-Butylcalix[4]arene Ligand, *Inorg. Chem.*, 2023, **62**, 401–407.

42 A. K. Das, S. Biswas, V. S. Wani, A. S. Nair, B. Pathak and S. Mandal, $[Cu_{18}H_3(S\text{-}Adm)_{12}(PPh_3)_4Cl_2]$: fusion of Platonic and Johnson solids through a Cu(0) center and its photophysical properties, *Chem. Sci.*, 2022, **13**, 7616–7625.

43 C.-F. Sun, N. Mammen, S. Kaappa, P. Yuan, G.-C. Deng, C.-W. Zhao, J.-Z. Yan, S. Malola, K. Honkala, H. Häkkinen, B. K. Teo and N.-F. Zheng, Thiolated Copper–Hydride Nanoclusters as Single-Site Hydrogenation Catalysts for Ketones in Mild Conditions, *ACS Nano*, 2019, **13**, 5975–5986.

44 H.-Y. Zhuo, H.-F. Su, Z.-Z. Cao, W. Liu, S.-A. Wang, L. Feng, G.-L. Zhuang, S.-C. Lin, M. Kurmoo, C.-H. Tung, D. Sun and L.-S. Zheng, High-Nuclear Organometallic Copper(I)-Alkynide Clusters: Thermochromic Near-Infrared Luminescence and Solution Stability, *Chem. – Eur. J.*, 2016, **22**, 17619–17626.

45 C. Gao, J. Wang, H. Xu and Y. Xiong, Coordination chemistry in the design of heterogeneous photocatalysts, *Chem. Soc. Rev.*, 2017, **46**, 2799–2823.

46 T.-T. Zhuang, Y. Liu, Y. Li, Y. Zhao, L. Wu, J. Jiang and S.-H. Yu, Integration of Semiconducting Sulfides for Full-Spectrum Solar Energy Absorption and Efficient Charge Separation, *Angew. Chem., Int. Ed.*, 2016, **55**, 6396–6400.

47 Z.-X. Yao, J.-Z. Li, H.-H. Wang, X. Cheng, L.-L. Hou, D.-N. Yu, D.-L. Chen, W.-Y. Dan and K.-G. Liu, Construction of eight mixed-valence pentanuclear $Cu^{I}_4Cu^{II}$ clusters using ligands with inhomogeneous electron density distribution: synthesis, characterization and photothermal properties, *Dalton Trans.*, 2022, **51**, 6053–6060.

48 X.-F. Chen, G.-H. Zhang, B. Li and L.-X. Wu, An integrated giant polyoxometalate complex for photothermally enhanced catalytic oxidation, *Sci. Adv.*, 2021, **7**, eabf8413.

49 J.-W. Zhang, L.-X. Wang, X. Cheng, L.-L. Hou, J.-Z. Li, C.-F. Wang, X.-W. Yan and K.-G. Liu, Use chloride to assist in constructing of penta- and nano-nucleus mixed-valent Cu(I/II) clusters and their photo-thermal properties, *Inorg. Chim. Acta*, 2023, **545**, 121270.

50 D.-X. Xu, Z.-D. Li, L.-S. Li and J. Wang, Insights into the Photothermal Conversion of 2D MXene Nanomaterials: Synthesis, Mechanism, and Applications, *Adv. Funct. Mater.*, 2020, 2000712.

 This journal is © the Partner Organisations 2023